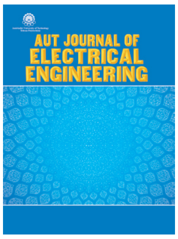

AUT Journal of Electrical Engineering

AUT J. Electr. Eng., 56(3) (2024) 453-464
DOI: 10.22060/eej.2024.23116.5590

The effect of a charge trap in the vicinity of the quantum-dot on the charge stability diagram of a single electron transistor

Fatemeh Hamedvasighi, Majid Shalchian*

Department of Electrical Engineering, Amirkabir University of Technology, Tehran, Iran

ABSTRACT: In this article, we explored the effect of a single charge trap on the charge stability diagram of the quantum-dot-based single-electron transistor. We investigated anomalies in the coulomb characteristic diagram, system energy, occupation probabilities, and quantum dot conductivity arising from the electrostatic interaction between the main dot and this charge trap. The anomalies were studied for various locations of the trap, mainly when the trap is located at the source or drain sides of the device. A significant enhancement in quantum dot conductivity was observed by bringing the main quantum dot closer to the source and drain with increased coupling capacitors. The trap, capacitively linked to the quantum dot, has two charge states, either empty or occupied by a single electron. Considering various quantum states, we solved the master equation using Fermi's golden rule to obtain tunneling rates and the matrix of tunneling coefficients. Inverting the coefficient matrix allowed us to determine the probability of each quantum state. The results of this analysis have been validated by comparing simulation results with experimental data. In conclusion, our study provides a valuable tool for detecting charge presence in a trap near a quantum dot, potentially applicable for the readout of quantum gates.

Review History:

Received: Apr. 15, 2024
Revised: May, 29, 2024
Accepted: Jun. 01, 2024
Available Online: Jul. 01, 2024

Keywords:

Single Electron Transistor
Quantum Dot
Coulomb Blockade
Trap
Charge Stability Diagram

1- Introduction

Electron transport mechanisms in single-electron systems, including quantum dots, dopant atoms, and single-electron transistors, represent a critical resource in the study of condensed matter physics. Additionally, established nanofabrication processes facilitate the systematic production of intricate assemblies of these single-electron entities. Such advancements are currently under investigation for their applicability in the construction of quantum computing architectures, highlighting their significance in the ongoing evolution of quantum technologies [1, 2]. Transport through single-electron systems involves phenomena such as Coulomb blockade, where the transport is suppressed unless a certain energy threshold is overcome. Quantum tunneling is crucial in allowing electrons to traverse potential barriers, enabling coherent transport at the nanoscale.

Usually, quantum point contacts (QPC) or single-electron transistors (SETs) are used to read single-electron charges or spins [3] in Qubits [4, 5]. These devices are sensitive to the electrostatic environment at certain gate-voltage biases, and the single-electron charging in the dot significantly changes its conductance, enabling single-electron charge sensing [6]. QPCs are narrow channels through which electrons can flow, and they are designed to exhibit quantized conductance due to the quantization of electron energy levels in one or more dimensions. The presence or absence of individual electrons passing through the QPC can be detected by carefully engineering the QPC and its surrounding environment. When the QPC captures an electron, it modifies the conductance of the QPC, leading to measurable changes in the electrical current. These changes can be detected and used as a signal to read out the charge state of the device [7, 8]. Using a QPC as a charge detector, the distribution function of current fluctuations in the QD can be directly measured by counting electrons. SETs have been used as very sensitive electrometers for the charge on a second quantum dot [9, 10]. Single-electron transistors (SETs) based on metallic tunnel junctions and gate-defined sensor quantum dots (SQD), conceptually equivalent to SETs, have also been widely used as proximal sensors and provide similar sensitivity and bandwidth [11-14]. In [15], mutual charge sensing between electron and hole quantum dots using a single electron transistor (SET) and a single-hole transistor (SHT) is reported. Both quantum dots sense charge displacement in the other quantum dots simultaneously. Moreover, [13] reports a real-time observation of an individual electron tunneling within a quantum dot, achieved through an integrated radio-frequency single-electron transistor (SET). Electron counting is employed to assess the quantum dot's tunneling frequency and the likelihood of its charge states being occupied.

Traps are one of the main factors that affect the electronic properties of QD-based devices [16, 17]. A system consisting

*Corresponding author's email: shalchian@aut.ac.ir

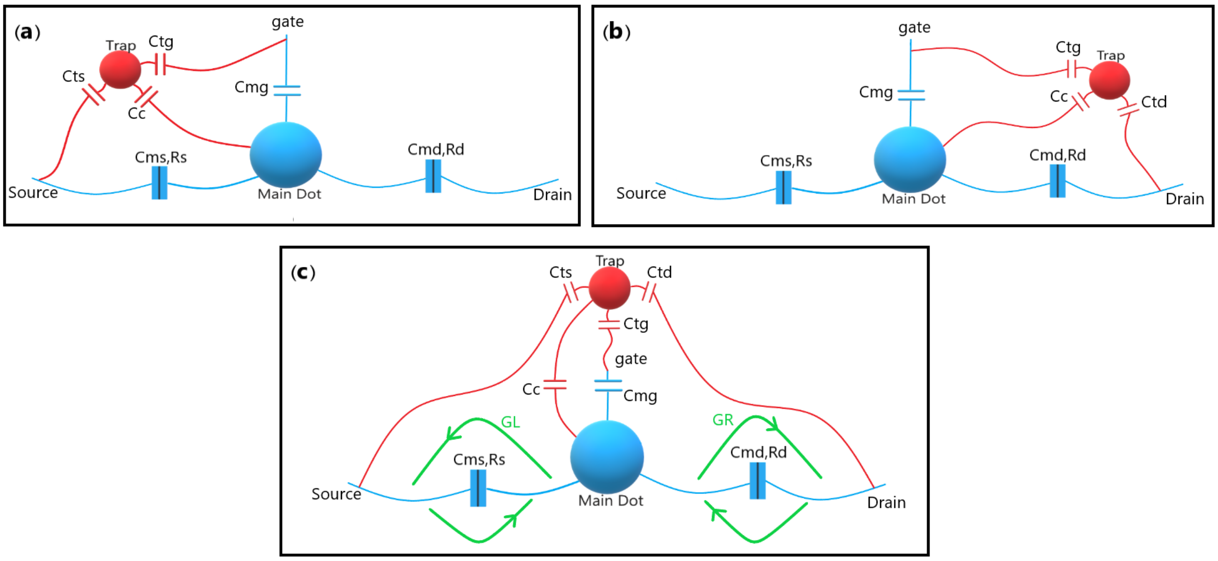

Fig. 1. Electrical model of the quantum dot in the vicinity of the trap [20] (a) The trap has a capacitive coupling to the source (b) The trap has a capacitive coupling to the drain (c) The trap has coupled to both source and drain

of a trap connected to a quantum dot is used for various purposes, such as qubit initialization, information storage, manipulation, electron-hole recombination, and limitation due to trapping states [18]. The trap may be intentionally placed in the system to limit and control the charge state of the quantum dot, which allows precise manipulation and measurement. It might also be located due to unavoidable factors such as lattice defects and deep impurities inside the structure [19] and near the main quantum dot. In both cases, there is a need to evaluate and analyze the effect of the trap and its charge state (full or empty) on the charge stability diagram of the quantum dot. By coupling the trap to the quantum dot, it is possible to control the energy levels and interactions of the quantum dot system, which promises applications in quantum information processing and quantum computing.

This work considers the effect of a charge trap, such as an isolated impurity, which is located in the vicinity of the main dot and capacitively coupled to it. We have taken into account the electrostatic interaction between the trap and the quantum dot. We analyzed the effect of trap position on the characteristic of the quantum dot.

There are usually two approaches to address the problem of interacting dots. One is based on classical coulomb blockade theory and capacitive coupling of the dota, which produce the principal features according to experimental results. This approach ignores quantum effects and spin interaction that slightly distort the charge stability diagram. Another approach is the quantum treatment based on the generalized Hubbard model. A generic numerical approach for solving the Master equation based on Hubbard Hamiltonian has been recently demonstrated for a double quantum dot system [3,22]. It takes into account spin-exchange, pair hopping, occupation-modulated hopping, and Zeeman splitting effects in the presence of an external magnetic field as well as the coulomb interaction. As demonstrated in [3], those effects slightly modify the shape and fade the boundaries of various regions in the charge stability diagram or create additional states within the regions such as singlet-triplet states which are beyond the scope of this work. However, the overall picture is the same as the classical approach.

In this work, we have used classical coulomb blockade theory and single-electron tunneling effect to calculate the tunneling rate from/to individual quantum states in the system using the master equation method and Fermi's golden rule. Finally, we have simulated anomalies in the characteristics of the quantum dot, which represents the charge state of the trap.

2- Device structure and parameters

Fig. 1 schematically shows the electrical model of the structure used in our simulation [20]. The main dot is between the source and drain leads, with two tunnel junctions. The gate electrode is coupled only capacitively (with zero tunneling probability) to the main dot (C_{mg}) and the trap (C_{tg}). As shown in Fig. 1. c, GL, and GR specify the tunneling rates between the main dot and the left and right leads.

The trap has been tested in three different positions, which are, respectively, the positions where the trap is capacitively coupled to the source (C_{ts}) and the quantum dot (C_c) (Fig. 1. a), the trap is capacitively coupled to the drain (C_{td}) and the quantum dot (C_c) (Fig. 1. b), and the trap is capacitively

Table 1. Coupling capacitances of the system used in the simulation

Capacitor	Value (aF)
C_{mg}	10
C_{md}	11
C_{ms}	11
C_{tg}	0.007
C_{ts}	0.3
C_{td}	0.3
C_c	0.25

coupled to both drain and source in addition to the quantum dot (Fig. 1. c). Table 1 lists the values of coupling capacitors specified in Fig. 1, which are obtained for an experimental structure [12]. The gate electrode controls the number of electrons in the quantum dot and the trap. The source and drain electrodes bias the device and establish a current through the source and drain tunnel junctions.

3- Electrostatic energy of the system

Fig. 2.a, obtained from [12], shows the system's electrostatic energy (W) in different charge states (E_0 for zero electrons in the trap and E_1 for one electron in the trap) as a function of gate voltage (V_g). To calculate the electrostatic energy, we assume that the number of electrons inside the quantum dot (n_m) can vary from 0 to 9, and the number of electrons inside the trap (n_t) can be 0 or 1. Therefore, there are ten different charge states as (0,0), (1,0), (2,0), ..., (9,0) in which the trap is empty and ten other charge states as (0,1), (1,1), (2,1), ..., (9,1) in which the trap is occupied by one electron and in general the system can have twenty different charge states.

The system's electrostatic energy W is calculated as a function of the charge in the quantum dot (Q_m) and the charge in the trap (Q_t):

$$W(Q_m,Q_t)=\frac{(Q_m+\beta_t Q_t+X)^2}{2C}+\frac{(Q_t+X_t)^2}{2(C_t+C_c)} \quad (1)$$

The parameters of the above relation are defined in (2) to (8). q_0 is the background charge in the dot.

$$Q_m(n_m)=-n_m q+q_0 \quad (2)$$

$$Q_t(n_t)=-n_t q \quad (3)$$

$$C_i=C_{is}+C_{id}+C_{ig} \quad (4)$$

C_i is the total coupling capacitances, including coupling to source, drain, and gate, where (i = m (for main dot) or t (for trap)).

$$\beta_t=\frac{C_c}{C_t+C_c} \quad (5)$$

$$C=C_m+\beta_t C_t \quad (6)$$

$$X_i=C_{is}V_s+C_{id}V_d+C_{ig}V_g \quad (7)$$

$$X=X_m+\beta_t X_t \quad (8)$$

Fig. 2.a shows the electrostatic energy of the system. Each parabola relates to a different value of n_m. The number of electrons in the dot increases due to the gate voltage increase. As shown in Fig. 2.b, when the system's energy is equal for both consecutive states, an electron is added to the quantum dot to decrease the system's energy. Blue parabola (E_0) shows the minimum energy (ground state) of the system for n_t=0, while black parabola (E_1) shows the minimum energy (ground state) of the system for n_t=1. For negative V_g, E_0 has lower energy and, therefore, is the favorite state of the system. By increasing the gate voltage, The system energy level in the E_0 state increases while the energy level for the E_1 state decreases; therefore, E_1 becomes more favorable than E_0, and the probability of trap charging increases. Fig. 3 shows the total system energy obtained from the simulation, calibrated

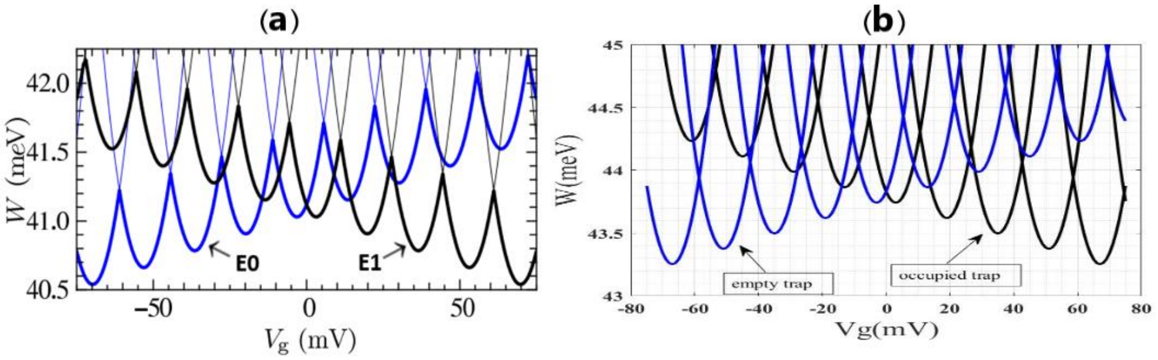

Fig. 2. Electrostatic energy of the system in different charge states at zero bias as a function of Vg (a) results from [20] (b) result of this work simulation in MATLAB

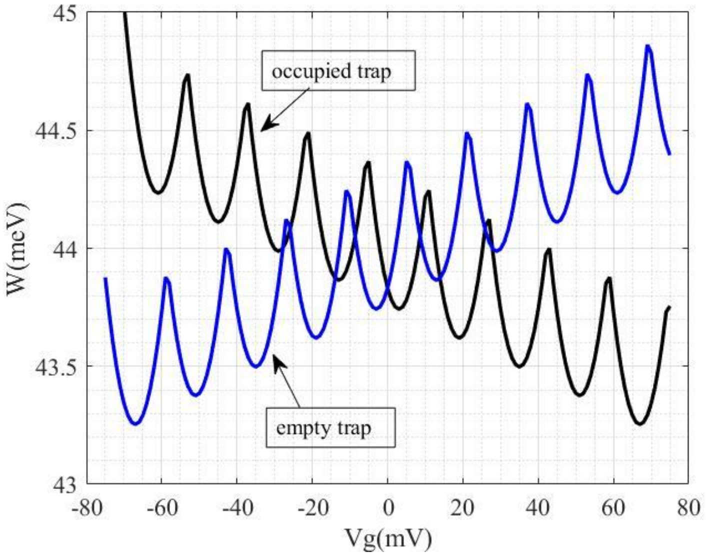

Fig. 3. The ground state energies of the main dot for the empty and occupied trap

with experimental data [20], by setting q_0 (background charge) as a fitting parameter.

4- Trap occupation and charge stability diagram

A common technique for simulating transport is the master equation approach [21, 22]. The aim is to determine the probability that a system occupies a given charge state in a steady state [23]. The system can have twenty different charge states, and the electrostatic energy of each state is described by (1). To calculate the tunneling rates, we calculate all possible transitions for each of these states to neighboring states. Fig. 4 shows all possible transitions among the system's charge states. The paths that are red and blue represent the transitions between the quantum dot and the source or drain leads, respectively, when the trap is empty and occupied, the paths in green represent the transitions between the leads and trap, and the paths in Black color represents transitions between quantum dot and trap.

The Fermi–Dirac distribution describes the occupation of the electron state. In this work, we have used the Fermi distribution function (9) to calculate the tunneling rates between the quantum dot and the trap and between the trap and the leads. We have also used Fermi-Dirac auto-convolution (10) to calculate the tunneling rates between the quantum dot and the leads due to the continuous nature of energy states on both sides of the transition [24].

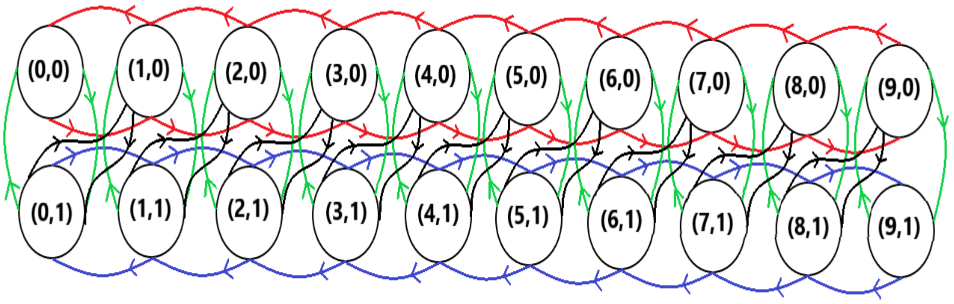

Fig. 4. All possible transitions among twenty different charge states of the system

$$f(x)=\frac{1}{e^{x}+1} \tag{9}$$

$$f^{*}(x)=(f*f)(x)=\frac{x}{e^{x}-1} \tag{10}$$

For example, we assume the system is initially in state (2,0). By adding an electron from the right or left leads (source or drain) to the quantum dot, the system moves to the (3,0) state, and conversely, by removing an electron from the quantum dot to the left or right leads, the system returns to state (2,0), in which the tunneling rates are according to relations (11) and (12) respectively.

$$G_{L,R(3,0),(2,0)}=T_1\,f^{*}\left(\frac{W_{(3,0)}-W_{(2,0)}+\mu_{L,R}}{K_BT}\right) \tag{11}$$

$$G_{L,R(2,0),(3,0)}=T_1\,f^{*}\left(\frac{W_{(2,0)}-W_{(3,0)}-\mu_{L,R}}{K_BT}\right) \tag{12}$$

In the above relations, the indices L and R represent the left and right electrodes; K_B is Boltzmann's constant, T_1 is a constant coefficient, which is 1000 times larger than T_2, considering that the capacitors connecting the quantum dot to the source and drain are much larger than the capacitors connecting the trap to the source and quantum dot and $\mu_{L,R}$ is the variation of the electrostatic energy of the system due to removing/adding a single electron from/to the left/right lead specified as (13):

$$\mu_{L,R}=-qV_{L,R} \tag{13}$$

In another case, an electron can be added to the trap from the left or right electrode, and as a result, the system moves from the (2,0) state to the (2,1) state, or vice versa, the electron inside the trap moves to the left or right electrodes, and the system returns from the state (2,1) to state (2,0), which are described in relations (14) and (15) respectively.

$$G_{L,R(2,1),(2,0)}=T_2\,f\left(\frac{W_{(2,1)}-W_{(2,0)}+\mu_{L,R}}{K_BT}\right) \tag{14}$$

$$G_{L,R(2,0),(2,1)}=T_2\,f\left(\frac{W_{(2,0)}-W_{(2,1)}-\mu_{L,R}}{K_BT}\right) \tag{15}$$

Finally, in the (2,0) state, an electron can tunnel from the quantum dot to the left or right electrode, and the system moves to the (1,0) state, or an electron can tunnel from the dot to the trap, and the system transits from the (2,0) state to the (1,1) state. Both of these tunnelings are also possible in reverse, that is, from the state (1,0) to (2,0) by adding an electron from the left or right electrode to the quantum dot and also from the state (1,1) to (2,0) by tunneling an electron from the trap to the quantum dot, all these tunnelings are shown in relations (16-19) respectively.

$$G_{L,R(1,0),(2,0)}=T_1\,f^{*}\left(\frac{W_{(1,0)}-W_{(2,0)}-\mu_{L,R}}{K_BT}\right) \tag{16}$$

$$G_{(1,1),(2,0)}=T_2\,f\left(\frac{W_{(1,1)}-W_{(2,0)}}{K_BT}\right) \tag{17}$$

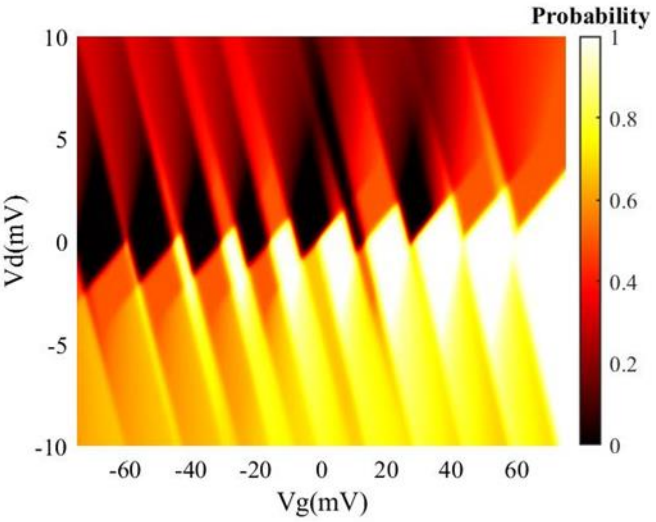

Fig. 5. Characteristics of source-coupled trap occupancy probability as a function of gate and drain voltage

$$G_{L,R(2,0),(1,0)} = T_1 f^*\left(\frac{W_{(2,0)} - W_{(1,0)} + \mu_{L,R}}{K_B T}\right) \tag{18}$$

$$G_{(2,0),(1,1)} = T_2 f\left(\frac{W_{(2,0)} - W_{(1,1)}}{K_B T}\right) \tag{19}$$

The net tunneling rate of (2,0) is obtained from the steady-state solution of the master equation. In other words, it is the difference between all the tunneling events leaving the (2,0) state and all the tunneling events entering the (2,0) state, as indicated in (20).

$$\begin{aligned}\Gamma_{(2,0)} &= G_{L,R(2,0),(1,0)} P_{(1,0)} + G_{(2,0),(1,1)} P_{(1,1)} \\ &+ G_{L,R(2,0),(2,1)} P_{(2,1)} + G_{L,R(2,0),(3,0)} P_{(3,0)} \\ &- P_{(2,0)} (G_{L,R(1,0),(2,0)} + G_{(1,1),(2,0)} \\ &+ G_{L,R(2,1),(2,0)} + G_{L,R(3,0),(2,0)})\end{aligned} \tag{20}$$

In (20), P(i,j) is the probability of charge state (i,j). After writing all the net tunneling rates for each state, the tunneling equations are written in matrix form using (21):

$$C = P\,A. \tag{21}$$

In relation (21), P is the vector of probabilities in the form of ($P_{(0,0)}$, $P_{(1,0)}$, $P_{(2,0)}$, …, $P_{(9,0)}$, $P_{(0,1)}$, $P_{(1,1)}$, $P_{(2,1)}$, …, $P_{(9,1)}$), A is the matrix of tunneling rates, which is obtained by taking into account the exchange of all states as we briefly demonstrated for (2,0) state, and C is a vector in the form of (c_1=0, c_2=0, c_3=0, …, c_{20}=1). The last equation indicates that the sum of probabilities of all charge states of the system should be unity.

Fig. 5 shows the collective probability for all states with one electron in the trap, which is coupled to the source (Fig. 1. a), including {(0,1),(1,1), …(9,1)} obtained from our calculations as a function of gate voltage and drain voltage. This figure shows a close correlation with Fig. 3. which suggests that the ground state of the system is an "Empty trap (E_0)" at V_g<-50 mV. It switches to "Occupied Trap" at V_g>50 mV, while the ground state oscillates between E_0 and E_1 as V_g varies in this range. Therefore, we expect the probability of trap occupation to also vary from 0 to 1 and show significant variations between 0 and 1 as we increase V_g. The tunneling current of the system is calculated by (22) :

$$\begin{aligned}I = -q \sum\nolimits_{n_m,n_t} &(G_{L(n_m+1,n_t)(n_m,n_t)} P_{(n_m,n_t)} \\ &+ G_{L(n_m,n_t+1))(n_m,n_t)} P_{(n_m,n_t)} \\ &- G_{L(n_m-1,n_t)(n_m,n_t)} P_{(n_m,n_t)} - G_{L(n_m,n_t-1)(n_m,n_t)} P_{(n_m,n_t)})\end{aligned} \tag{22}$$

Fig. 6 shows the tunneling conductance (a derivative of the tunneling current) as a function of V_d and V_g. The conductance curve is usually referred to as the charge stability diagram, and our simulation results (Fig 6. b) show excellent

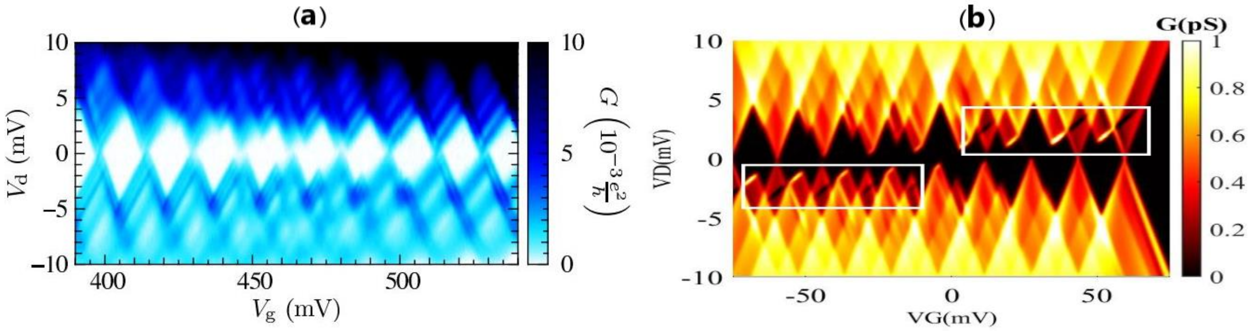

Fig. 6. Conductance characteristic of a quantum dot in the vicinity of an occupied source-coupled trap (a) Experimental results [12] (b) result of this work simulation in MATLAB

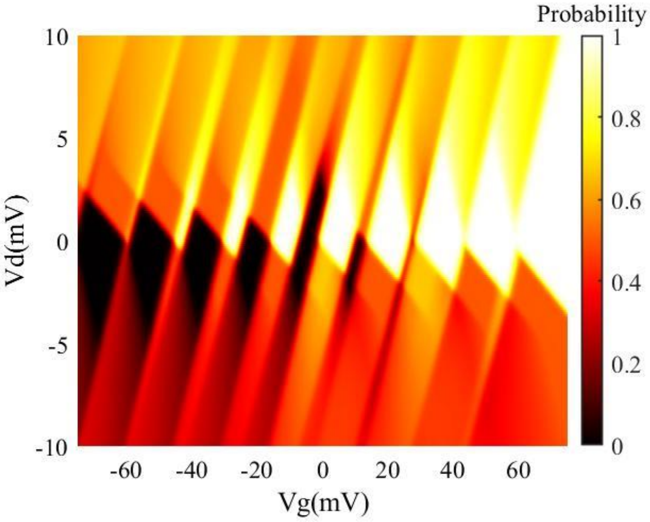

Fig. 7. Characteristics of drain-coupled trap occupancy probability as a function of gate and drain voltage

agreement with the experimental data (Fig 6. a [12]). The anomalies of the charge stability diagram are compared with the diagram of an ideal single-electron transistor (simple diamond shape) and are the footprint of the charged trap.

When the trap is located at the drain side and coupled to the drain, the probability of trap occupation increases by increasing the drain voltage. This feature is demonstrated in Fig. 7, which shows horizontal mirror characteristics compared to Fig. 5, where the trap is located at the source side.

Another distinctive feature for source-side and drain-side traps is extra teeth, demonstrated in the charge stability diagram of Fig. 6.b for the source-side trap and Fig. 8 for the drain-side trap, highlighted with white boxes. According to Fig. 6. b, when the traps are at the source side, these extra teeth are more visible if the gate voltage and the drain voltage are both positive or negative, but this feature is mirrored again for the drain-side trap.

Fig. 9 shows the trap's occupation probability when capacitively connected to both the source and the drain (Fig. 1.c). This structure equals the intersection of the probabilities of occupation for the trap connected to the source (Fig. 5) and the trap connected to the drain (Fig.7). This causes the creation of triangular shapes (symmetric in the y-direction), which become brighter with increasing the gate voltage, as the probability of occupancy increases.

Fig. 10 shows the conductance characteristics of a trap coupled to the source, drain, and gate. It shows that the probability of the trap filling is almost uniform for positive and negative drain biases; therefore, extra teeth are found throughout the characteristic.

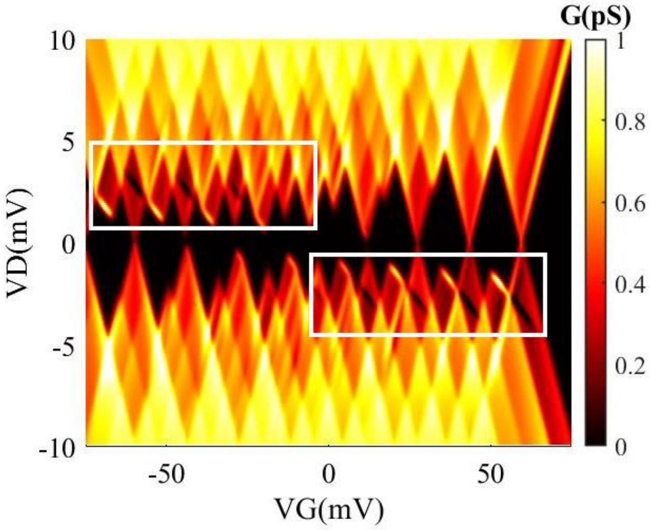

Fig. 8. Conductance characteristic of a quantum dot in the vicinity of an occupied drain-coupled trap

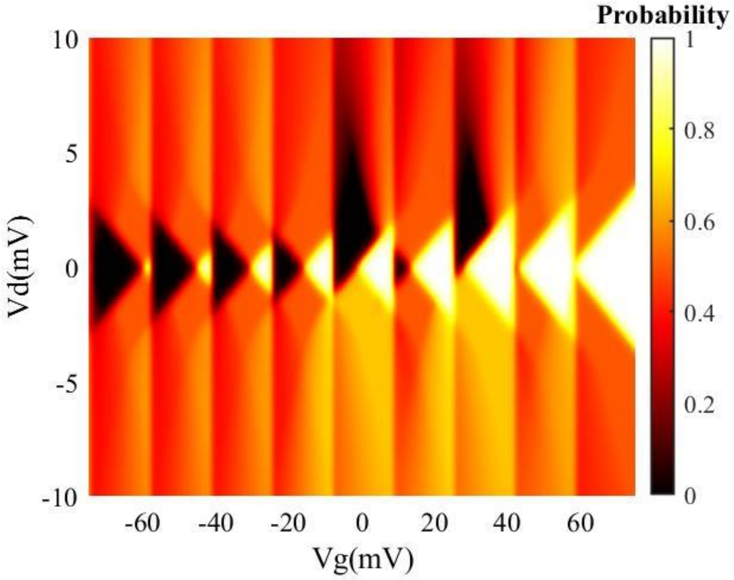

Fig. 9. Characteristics of source and drain-coupled trap occupancy probability as a function of gate and drain voltage

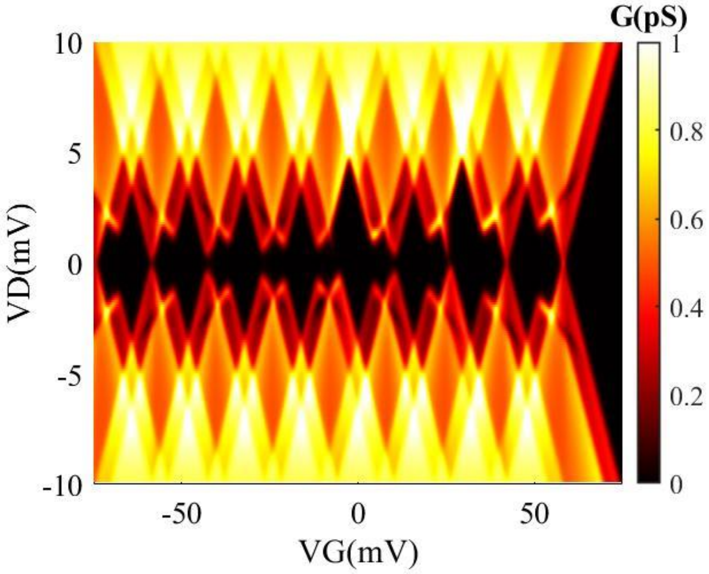

Fig. 10. Conductance characteristic of a quantum dot in the vicinity of an occupied source and drain-coupled trap

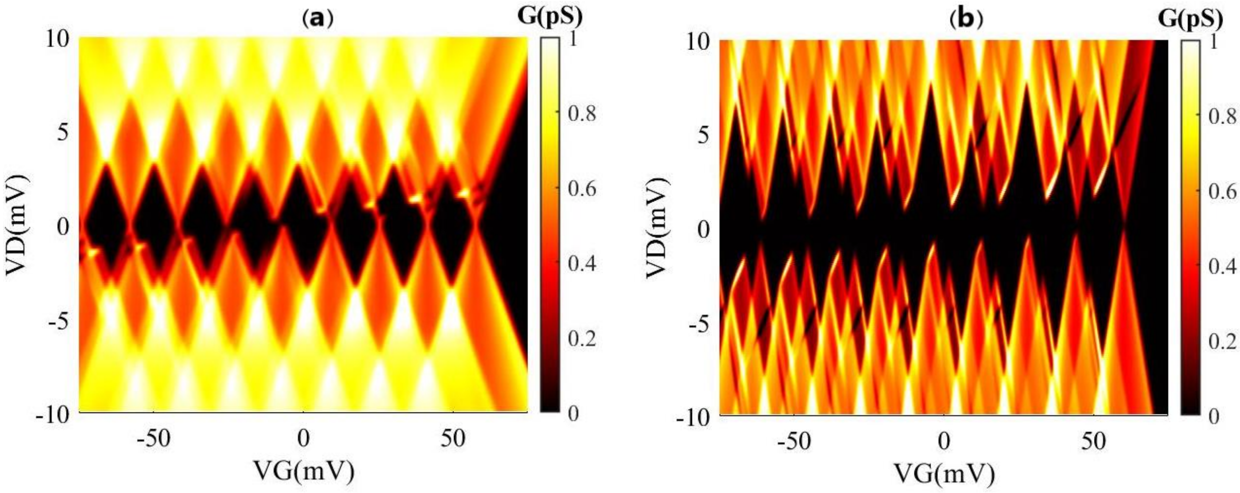

Fig. 11. Conductivity characteristic of a quantum dot in the vicinity of a trap (a) Quantum dot has strong coupling with source and drain and weak coupling with trap (b) Quantum dot has weak coupling with source and drain and strong coupling with trap

5- Dot-Lead-Trap coupling strength

The stronger coupling enhances the interaction between the quantum dot and the leads or trap, facilitating the transfer of electrons, resembling the dot's movement toward the leads or trap. Conversely, when the coupling capacitors are decreased, the interaction between the quantum dot and the leads or trap reduces, resembling the dot's movement away from the leads or trap.

Fig. 11 shows the quantum dot charge stability diagram near the trap in different states. In the first case (Fig. 11.a), we increased the coupling capacitor between the quantum dot and the source and drain leads to 18 aF and decreased the coupling capacitor between the quantum dot and the trap to 0.08 aF. In this case, the conductivity has increased (in the range of 0.6 to 1 mA), and the anomaly (extra teeth) of the diagram due to trap perturbation is reduced. In the second case (Fig. 11.b), we reduced the coupling capacitors between the quantum dot and the leads to 5 aF and increased the

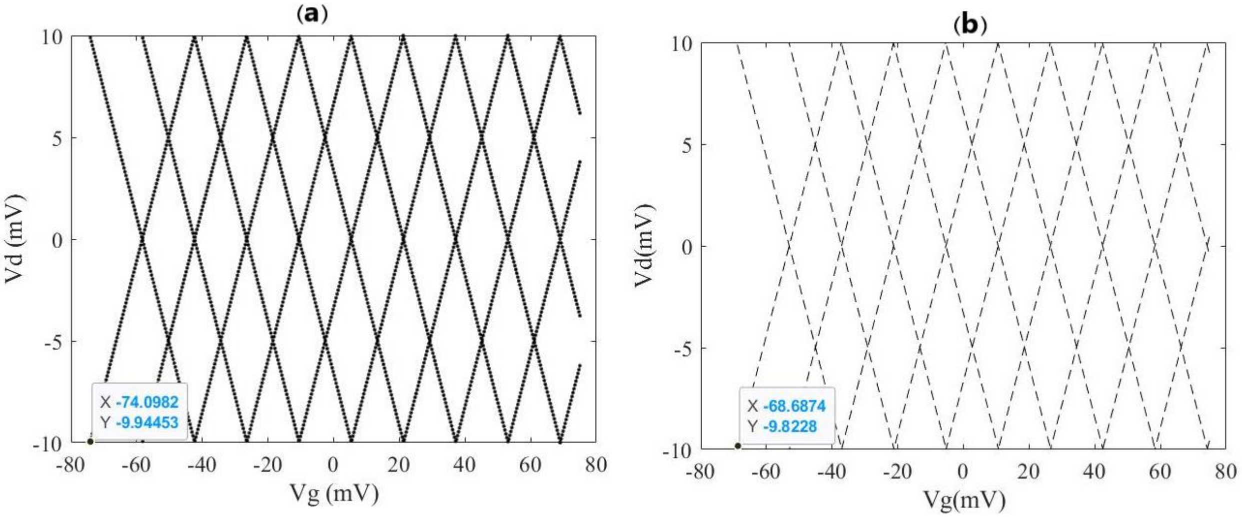

Fig. 12. Coulomb characteristic diagram of a quantum dot in the vicinity of a trap (a) When the trap is empty (b) When the trap is occupied

coupling between the quantum dot and the trap to 0.35 aF. As can be seen, the conductivity decreased (in the range of 0 2 to 0.6 mA), and additional teeth were observed due to the disturbance induced by the trap.

6- Shift of the dot coulomb blockade characteristic due to trap charging

Fig. 12 shows the boundaries of neighboring charge states of the main dot in the V_g and V_d plane for two scenarios: a) empty trap and b) occupied trap. As can be seen, there is a horizontal shift of 5.4mV in Fig 12. b compared to Fig 12.a. This shift can be attributed to the coulombic repulsion between the charged trap and the electrons in the main dot, which leads to additional energy (gate voltage) required to add a single electron to the main dot. By increasing the capacitor between the trap and the gate (C_{tg}), the horizontal shift decreases because by increasing the coupling between the trap and the gate and by increasing the gate voltage, the effect of the gate on the presence of electrons in the trap rises, and as a result, the impact of electron repulsion at the main point with the trap decreases, and less shift is created.

7- Conclusion

This work has studied the effect of a charge trap near the quantum dot on the charge stability diagram. Several scenarios have been investigated, including the situation when the two-state trap is coupled with source, drain, and both source and drain. Tunneling rates were calculated using the master equation for all permitted transitions with neighboring states, and the matrix of tunneling coefficients was obtained. The current diagram, conduction, and Coulomb blockade characteristics were simulated in MATLAB for both empty and occupied traps, and the simulation results are in good agreement with the experimental results. The presence of the trap with different charge states results in the anomaly of the pure SET diamond characteristics in the form of extra teeth and a shift of stability diagram; these features might be used to estimate the location and coupling strength between the dot, trap, and the leads. Furthermore, this analysis might intentionally position a trap near a qubit for manipulation and readout of the charge state of the main dot for quantum computing applications.

8- Acknowledgements

The authors would like to thank Dr. Farzan Jazaeri from EPFL for technical discussions and Dr. Amin Rassekh for sharing his work on double quantum dots.

9- Nomenclature

C_{mg}	The capacitor between the quantum dot and the gate, F
C_{md}	The capacitor between the quantum dot and the drain, F
C_{ms}	The capacitor between the quantum dot and the source, F
C_{tg}	The capacitor between the trap and the gate, F
C_{ts}	The capacitor between the trap and the source, F
C_{td}	The capacitor between the trap and the drain, F
C_c	The capacitor between the trap and the quantum dot, F

C_t	Capacitors connected to the trap, F
C	Total system capacitors, F
W	Electrostatic energy, J
Qm/t	The charge in the quantum dot/ trap, C
nm/t	The number of electrons in the quantum dot/ trap
X	Charge stored in all system capacitors, J
X_t	Charge stored in capacitors connected to the trap, J
X_m	Charge stored in capacitors connected to the quantum dot, J
q_0	The background charge in the dot, C
q	absolute value of the electron charge, $1.602.10^{-19}$ C
$V_g/ V_s/ V_d$	Gate/ Source/ Drain voltage, V
e	Euler's number, 2.718
$G_{L,R}$	Tunneling rate between two consecutive states to/ from left or right leads
T_1, T_2	Constant coefficients 1, 1000
K_B	Boltzmann factor, $1.381.10^{-23}$ J/k
T	Temperature, K
$V_{L,R}$	The voltage of the left or right leads, V
P	The vector of probabilities
A	The matrix of tunneling rate

Greek symbols

β_t	Structure of the trap signature
$\mu_{L,R}$	Chemical potential in left or right leads, J
Γ	The net tunneling rate of a state

Subscript

m	Quantum dot
t	Trap
L	Left
R	*Right*

References

[1] M. Veldhorst, H. Eenink, C.-H. Yang, and A. S. Dzurak, "Silicon CMOS architecture for a spin-based quantum computer," Nature communications, vol. 8, no. 1, p. 1766, 2017.

[2] C. H. Yang et al., "Operation of a silicon quantum processor unit cell above one kelvin," Nature, vol. 580, no. 7803, pp. 350-354, 2020.

[3] A. Rassekh, M. Shalchian, J.-M. Sallese, and F. Jazaeri, "Design space of quantum dot spin qubits," Physica B: Condensed Matter, vol. 666, p. 415133, 2023.

[4] B. E. Kane, "A silicon-based nuclear spin quantum computer," nature, vol. 393, no. 6681, pp. 133-137, 1998.

[5] D. Loss and D. P. DiVincenzo, "Quantum computation with quantum dots," Physical Review A, vol. 57, no. 1, p. 120, 1998.

[6] H. Kiyama et al., "Single-electron charge sensing in self-assembled quantum dots," Scientific reports, vol. 8, no. 1, p. 13188, 2018.

[7] S. Gustavsson et al., "Counting statistics of single electron transport in a quantum dot," Physical review letters, vol. 96, no. 7, p. 076605, 2006.

[8] Y. Yin, "Emission rate of electron transport through a quantum point contact," Journal of Physics: Condensed Matter, vol. 35, no. 35, p. 355301, 2023.

[9] P. Lafarge, H. Pothier, E. R. Williams, D. Esteve, C. Urbina, and M. H. Devoret, "Direct observation of macroscopic charge quantization," Zeitschrift für Physik B Condensed Matter, vol. 85, pp. 327-332, 1991.

[10] L. Molenkamp, K. Flensberg, and M. Kemerink, "Scaling of the Coulomb energy due to quantum fluctuations in the charge on a quantum dot," Physical review letters, vol. 75, no. 23, p. 4282, 1995.

[11] T. Buehler et al., "Single-shot readout with the radio-frequency single-electron transistor in the presence of charge noise," Applied Physics Letters, vol. 86, no. 14, 2005.

[12] T. Fujisawa, T. Hayashi, Y. Hirayama, H. Cheong, and Y. Jeong, "Electron counting of single-electron tunneling current," Applied physics letters, vol. 84, no. 13, pp. 2343-2345, 2004.

[13] W. Lu, Z. Ji, L. Pfeiffer, K. West, and A. Rimberg, "Real-time detection of electron tunnelling in a quantum dot," Nature, vol. 423, no. 6938, pp. 422-425, 2003.

[14] R. Schoelkopf, P. Wahlgren, A. Kozhevnikov, P. Delsing, and D. Prober, "The radio-frequency single-electron transistor (RF-SET): A fast and ultrasensitive electrometer," science, vol. 280, no. 5367, pp. 1238-1242, 1998.

[15] A. S. de Almeida et al., "Ambipolar charge sensing of few-charge quantum dots," Physical Review B, vol. 101, no. 20, p. 201301, 2020.

[16] D. Bozyigit, S. Volk, O. Yarema, and V. Wood, "Quantification of deep traps in nanocrystal solids, their electronic properties, and their influence on device behavior," Nano letters, vol. 13, no. 11, pp. 5284-5288, 2013.

[17] A. A. Cordones and S. R. Leone, "Mechanisms for charge trapping in single semiconductor nanocrystals probed by fluorescence blinking," Chemical Society Reviews, vol. 42, no. 8, pp. 3209-3221, 2013.

[18] A. H. Ip et al., "Hybrid passivated colloidal quantum dot solids," Nature nanotechnology, vol. 7, no. 9, pp. 577-582, 2012.

[19] S. C. Boehme et al., "Density of trap states and Auger-mediated electron trapping in CdTe quantum-dot solids," Nano Letters, vol. 15, no. 5, pp. 3056-3066, 2015.

[20] M. Hofheinz, X. Jehl, M. Sanquer, G. Molas, M. Vinet, and S. Deleonibus, "Individual charge traps in silicon nanowires: Measurements of location, spin and

occupation number by Coulomb blockade spectroscopy," The European Physical Journal B-Condensed Matter and Complex Systems, vol. 54, pp. 299-307, 2006.

[21] S. Datta, Quantum transport: atom to transistor. Cambridge university press, 2005.

[22] A. Rassekh, M. Shalchian, J.-M. Sallese, and F. Jazaeri, "Tunneling Current Through a Double Quantum Dots System," Ieee Access, vol. 10, pp. 75245-75256, 2022.

[23] R. A. Bush, E. D. Ochoa, and J. K. Perron, "Transport through quantum dots: An introduction via master equation simulations," American Journal of Physics, vol. 89, no. 3, pp. 300-306, 2021.

[24] M. Hofheinz, "Coulomb blockade in silicon nanowire MOSFETs," Université Joseph-Fourier-Grenoble I, 2006.

HOW TO CITE THIS ARTICLE

F. Hamedvasighi, M. Shalchian. The effect of a charge trap in the vicinity of the quantum-dot on the charge stability diagram of a single electron transistor . AUT J Electr Eng, 56(3) (2024) 453-464.

DOI: 10.22060/eej.2024.23116.5590